

Correlating off-stoichiometric doping with nanoscale electronic disorder and quasiparticle interference pattern in high- T_c superconductor $\text{Bi}_2\text{Sr}_2\text{CaCu}_2\text{O}_{8+\delta}$

Sen Zhou, Hong Ding, and Ziqiang Wang

Department of Physics, Boston College, Chestnut Hill, MA 02467

(Dated: April 24, 2017)

A microscopic theory is presented for the observed electronic disorder in superconducting $\text{Bi}_2\text{Sr}_2\text{CaCu}_2\text{O}_{8+\delta}$. The essential phenomenology is shown to be consistent with the existence of two types of interstitial oxygen dopants: those serving primarily as charge reservoirs and those close to the apical plane contributing both carriers and electrostatic potential to the CuO_2 plane. The non-linear screening of the latter produces nanoscale variations in the doped hole concentration, leading to electronic inhomogeneity. Based on an unrestricted Gutzwiller approximation of the extended t - J model, we provide a consistent explanation of the correlation between the observed dopant location and the pairing gap and its spatial evolutions. We show that the oxygen dopants are the primary cause of both the pairing gap disorder and the quasiparticle interference pattern.

PACS numbers: 71.27.+a, 71.18.+y, 74.25.Jb, 74.70.-b

Remarkable electronic inhomogeneities have been observed by scanning tunneling microscopy (STM) in high- T_c superconductors $\text{Bi}_2\text{Sr}_2\text{CaCu}_2\text{O}_{8+\delta}$ [1, 2, 3, 4, 5], $\text{Ca}_{2-x}\text{Na}_x\text{CuO}_2\text{Cl}_2$ [6, 7], and $\text{Bi}_{2-x}\text{Pb}_x\text{Sr}_2\text{CuO}_y$ [8] over a wide range of doping. The hallmark of the inhomogeneity is the disordered, nanometer scale variation of the pairing energy gap and its anti-correlation with that of the coherence peak height in the local density of states (LDOS). The origin of the electronic disorder has been the focus of several theoretical studies [9, 10, 11, 12, 13]. It was emphasized [1, 9, 10] that off-stoichiometric doping a Mott insulator, such as the high- T_c cuprates, creates inherently inhomogeneous electronic states associated with the interstitial or substitutional dopant atoms. Ionized, these off-plane dopants act as disordered centers of nonlinearly screened electrostatic potential, leading to a spatially inhomogeneous distribution of the local doping concentration (LDC) and hence that of the local pairing gap. In a short coherence length superconductor described by the short-range resonance valence bond theory [15, 16], the local pairing gap is anti-correlated with the LDC [9, 10].

The notion of dopant induced electronic disorder is supported and further advanced by the recent STM experiments of McElroy et.al. [4]. Identifying the spectral peak around -0.96eV in the LDOS with the presence of a local excess oxygen atom, the correlation between the dopant location and the gap inhomogeneity has been established ubiquitously. However, the observed dopants reside close to the regions of large pairing gap. This is counter-intuitive since the negatively charged oxygen ions are expected to attract nearby holes and create a higher LDC with a smaller pairing gap [9, 10]. This discrepancy promotes the idea that dopant induced local structural distortions may play a more important role than potential disorder [4, 17] and phenomenological theories in which the dopants serve as large pairing centers [13]. The origin of the dopant induced electronic disorder

has remained a central unresolved issue.

In this paper, we show that, while dopant induced structural effects are present, the main cause for the electronic disorder is the dopant potential induced LDC modulations. A clue as to how the latter can be consistent with the dopant locations comes from the following observations made on the experiments of McElroy et.al. [4]: (1) The observed dopants associated with the -0.96eV peak cannot account for the total number of oxygen dopants. For example, in the underdoped sample with $\bar{\Delta} = 65\text{meV}$, the observed dopant density is 2.7%. Even if every oxygen dopant is fully ionized, the average doping would only be 5.5%, which is much smaller than the expected value around 11% [14]. Thus, a substantial number of the dopants has not been located, too large to be accounted for by the uncertainty in the doping process. (2) The correlation between the observed dopants and the pairing gap is weak and well defined only in the statistical sense. An appreciable number of them can be found in the smaller gap regions or to straddle the boundaries between the small and large gap regions. Thus, it is unlikely that the observed dopants strongly and directly affect the *local* electronic structure. (3) The in-gap, low energy states in the LDOS have their weight concentrated in regions away from the identified dopants. This suggests that these electronic states which are encoded with the quasiparticle interference modulations [4] are likely localized or pinned by additional confining potentials in regions away from the identified dopants.

Based on these observations, we conjecture that there are two types (A and B) of interstitial oxygen dopants in $\text{Bi}_2\text{Sr}_2\text{CaCu}_2\text{O}_{8+\delta}$. The type-B dopants serve primarily as charge reservoirs. They only couple weakly to the CuO_2 plane. These near nonbonding oxygen orbitals give rise to the -0.96eV peak in the LDOS [4]. Recent ARPES measurements show that the dopant induced states near -0.96eV have B_1 symmetry and do not mix with the doped holes residing in the planar orbitals

[18]. This further supports the identification of the former with the type B-dopants. The type-A dopants, on the other hand, strongly affect the local electronic structure in the CuO_2 plane. Their electrostatic potential enhances the LDC which in turn pushes the orbital energy of type-A dopants into the broad valence band spectra below -1.2eV not yet accessible by STM probes. One possibility is that the type-B dopants sit above the BiO plane while type-A dopants come close to the apical SrO layer. We will discuss the microscopic origin of the latter at the end.

To support this physical picture, we extend the t - J model to include the oxygen dopant potential,

$$H = - \sum_{i \neq j} t_{ij} P c_{i\sigma}^\dagger c_{j\sigma} P + J \sum_{\langle i,j \rangle} (\mathbf{S}_i \cdot \mathbf{S}_j - \frac{1}{4} \hat{n}_i \hat{n}_j) + \sum_{i \neq j} \hat{n}_i V_{ij}^c \hat{n}_j - \sum_i (V_i^A + V_i^B) (1 - \hat{n}_i). \quad (1)$$

Here $c_{i\sigma}^\dagger$ creates an electron that hops between near neighbors of the Cu square lattice via t_{ij} . Repeated spin indices are summed and $\hat{n}_i = c_{i\sigma}^\dagger c_{i\sigma}$ is the density operator. The LDC is given by $x_i = 1 - n_i$, $n_i = \langle c_{i\sigma}^\dagger c_{i\sigma} \rangle$. The average doping will be denoted as $\delta = (1/N_s) \sum_i x_i$ on a lattice of N_s sites. The second line in Eq. (1) describes the long-range Coulomb interactions between the electrons in the plane and between the in-plane doped holes and the two-types of off-plane dopants, $V_{ij}^c = V_c/|r_i - r_j|$ and

$$V_i^{A(B)} = \sum_{\ell_{A(B)}=1}^{N_{A(B)}} \frac{2V_{A(B)}}{\sqrt{|r_i - r_{\ell_{A(B)}}|^2 + d_{A(B)}^2}} \quad (2)$$

where d_A, d_B are the setback distances and N_A, N_B the number of type-A and type-B dopants respectively, $\delta = 2(N_A + N_B)/N_s$.

Eq. (1) describes doped Mott insulators because of the projection operator P that removes double occupation. The projection is most conveniently implemented using the Gutzwiller approximation by the statistical weighting factors multiplying the coherent states, thus renormalizing the hopping and the exchange parameters [20]. Since the dopants break translation symmetry, we extend the approach to the disordered case by the renormalization $t_{ij} \rightarrow g_{ij}^t t_{ij}$ and $J \rightarrow g_{ij}^J J$ where the Gutzwiller factors

$$g_{ij}^t = \sqrt{\frac{4x_i x_j}{(1+x_i)(1+x_j)}}, \quad g_{ij}^J = \frac{4}{(1+x_i)(1+x_j)} \quad (3)$$

depend on the local doping at the sites connected by the hopping and the exchange processes. The exchange term is decoupled in terms of the bond $\chi_{ij} = \langle c_{i\sigma}^\dagger c_{j\sigma} \rangle$ and the pairing $\Delta_{ij} = \langle \epsilon_{\sigma\sigma'} c_{i\sigma} c_{j\sigma'} \rangle$ fields, leading to a renormalized mean-field Hamiltonian,

$$H_{\text{GA}} = - \sum_{i \neq j} g_{ij}^t t_{ij} c_{i\sigma}^\dagger c_{j\sigma} + \sum_i \epsilon_i c_{i\sigma}^\dagger c_{i\sigma}$$

$$- \frac{1}{4} J \sum_{\langle i,j \rangle} g_{ij}^J [\Delta_{ij}^* \epsilon_{\sigma\sigma'} c_{i\sigma} c_{j\sigma'} + \chi_{ij}^* c_{i\sigma}^\dagger c_{j\sigma} + \text{h.c.}] + \frac{1}{4} J \sum_{\langle i,j \rangle} g_{ij}^J (|\Delta_{ij}|^2 + |\chi_{ij}|^2) - \sum_i \lambda_i n_i. \quad (4)$$

The local energy for the electrons is given by $\epsilon_i = V_{\text{sc}}(i) + \lambda_i - \mu_f$, where μ_f is the chemical potential and λ_i is a fugacity that, together with the last term, ensures the equilibrium condition under local occupation $\langle c_{i\sigma}^\dagger c_{i\sigma} \rangle = n_i$ [21]. $V_{\text{sc}}(i)$ is the screened Coulomb potential,

$$V_{\text{sc}}(i) = V_i^A + V_i^B + V_c \sum_{j \neq i} \frac{x_i - \delta}{|r_i - r_j|}. \quad (5)$$

This is the driving force of the electronic disorder through local doping variations. The correlation of the latter to the local pairing gap disorder is caused by the Gutzwiller factor g^t in Eq. (3) that modulates the kinetic energy locally. Minimizing the ground state energy of Eq. (4), we obtain the self-consistent equations for the set of parameters $(\Delta_{ij}, \chi_{ij}, \lambda_i, x_i, \mu_f)$, which are solved iteratively for a given average doping δ .

We present our results for systems of 32×32 sites. We use $t_{ij} = (0.48, -0.16, 0.05, 0.05, -0.05)\text{eV}$ and $J = 0.08\text{eV}$ such that the quasiparticle dispersion in Eq. (4) agrees with that measured by angle-resolved photoemission [19]. For simplicity, half of the dopants are taken to be B-type and the other half A-type distributed randomly with $d_A = 1a$. The bare electrostatic potentials are set to $V_A = V_c = 0.5\text{eV}$, and $V_B = 0$ for the weak coupling between B-dopants and doped holes. Note that the locations of type-A and type-B dopants are *naturally anticorrelated* over the average interdopant distance $a\sqrt{2}/\delta$. The spatial distribution of the LDC x_i and the d-wave pairing order parameter $\Delta_d(i)$ are shown as 2D maps in Figs. 1a and 1b for a typical system at $\delta = 10.2\%$. The projected dopant locations are superimposed. The A-dopants are ubiquitously correlated with the LDC. Due to the local pairing nature of the short-range RVB state, x_i is in turn strongly anticorrelated with $\Delta_d(i)$ [9]. Notice that the modulations induced by the A-dopants leaves the B-dopants unwittingly correlated overall with the low doping and strong pairing regions. The LDOS is calculated from the projected retarded Green's function in the Gutzwiller approximation [21], $\text{LDOS}(i, \omega) = -2\text{Im}g_{ii}^t G(i, i, \omega + i0^+)$. To reduce finite size effects, we average over different boundary conditions corresponding to 20×20 supercells. As in the STM experiments, the local tunneling gap Δ_T is extracted from the coherence peak position at positive bias in the LDOS. In Fig. 1c, the tunneling gap map is shown with the dopant locations. Evidently, Δ_T is small near the A-dopants where the LDC is high. Notice however, that the B-dopants are found with high statistics in and around the regions where the tunneling gap is large, consistent with their identification with those observed

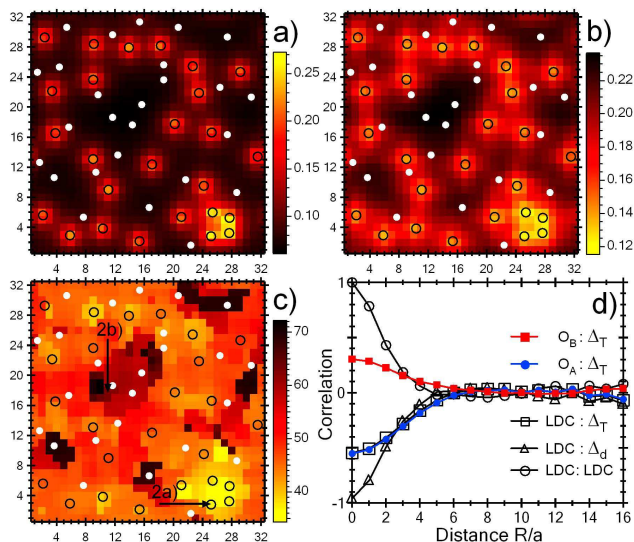


FIG. 1: Doping and pairing disorder on a 32×32 system at $\delta = 10.2\%$. 2D maps are shown for the LDC x_i (a), dimensionless d-wave pairing order parameter Δ_d (b), and tunneling gap Δ_T in meV (c) with the projected type-A (open black circle) and type-B (white solid circle) dopant locations superimposed. (d) Correlation functions among the dopant location, Δ_T , x_i , and Δ_d .

by STM [4]. To elucidate the correlation between the dopants and electronic disorder, we calculate the normalized cross-correlation function between the dopants and the tunneling gap,

$$C_{\Delta_T-O_{A(B)}}(r_j) = \frac{\sum_i \delta\Delta_T(r_i)\delta O_{A(B)}(r_i + r_j)}{\sqrt{\sum_i [\delta\Delta_T(r_i)]^2 \sum_j [\delta O_{A(B)}(r_j)]^2}}$$

where $\delta f(r_i) = f(r_i) - \langle f \rangle$. The dopant locations are modeled by Lorentzians of width $2a$ [4]. Fig. 1d shows that, while Δ_T is strongly anticorrelated with A-dopant locations ($C_{\Delta_T-O_A}(0) \sim -0.6$), the B-dopants (observed by STM) are positively correlated with the local tunneling gap, and moreover, the correlation is significantly weaker, $C_{\Delta_T-O_A}(0) \sim 0.3$, in excellent agreement with experiments [4].

The large LDC variation is not inconsistent with the STM integrated LDOS variation that diminishes only when integrated up to -0.6eV to -0.9eV , where large incoherent background and the spectral weight associated with the dopants contribute appreciably [4]. It is a subtle task to relate quantitatively the integrated LDOS or the topography to the LDC since the former are obtained in the constant tunneling current mode where the tip to sample distance changes significantly, leading to reduced spatial variations of the spectral weight [1, 9].

This form of dopant induced electronic disorder can describe the basic properties of the inhomogeneous low energy states observed experimentally. In Fig. 2, we present the LDOS along the two line-cuts indicated in Fig. 1c.

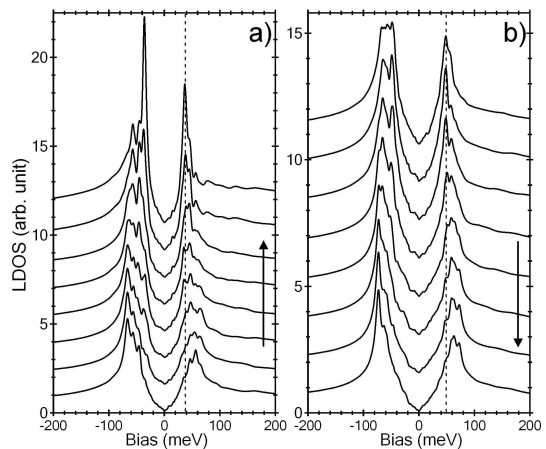


FIG. 2: Evolutions of the LDOS along two line cuts (shown in Fig. 1c) from small to average (a) and average to large (b) gap regions. Dashedlines are guide to eye.

Clearly, larger (smaller) gap regions are associated with smaller (larger) coherence peaks in agreement with STM [1, 2, 3, 4, 5]. Note that the line-cut passes through locally highly overdoped regions with $x_i > 25\%$. In a uniform system, the pairing gap would be vanishingly small and the system essentially in the normal state at such high doping levels. Fig. 2a and Fig. 1c show, however, that the smaller local gap is still sizable. That overdoped regions of sizes not exceeding the coherence length have gap values considerably above those in a clean sample at the corresponding dopings was first pointed out in Ref.[9], and is likely a manifestation of the proximity effect due to the surrounding larger gap regions. Indeed, Fig. 2 shows that as we move away from the small (large) gap region, a larger (smaller) gap emerges and evolves progressively stronger until it becomes the dominant gap as the line cut enters the lower (higher) doping region. This feature has been observed recently by STM with high energy resolutions [5].

Next we show the A-dopants, the culprit of strong gap disorder, also serve as the primary cause of the low-energy quasiparticle interference modulations [22]. In Fig. 3a, the 2D maps of the LDOS(i, ω) is plotted at fixed energies ω , showing different interference patterns. The maxima of the spatial modulations are preferentially centered around the A-dopant sites, thus away from the B-dopants, consistent with STM observations. This turns out to be true for all low energy states. In Fig. 3c, we plot the *local* correlation between the LDOS and the dopant locations as a function of bias voltage. For both positive and negative energies, the correlations are positive and strong (reaching 0.9) with A-dopants and negative (anticorrelated) and weak (reaching -0.3) with B-dopants. The peak and dip around $\pm 70\text{meV}$ are related to the Van Hove-like feature in the LDOS spectra seen in Fig. 2. Just as in the case of dopant-gap correlations, the strong *cor-*

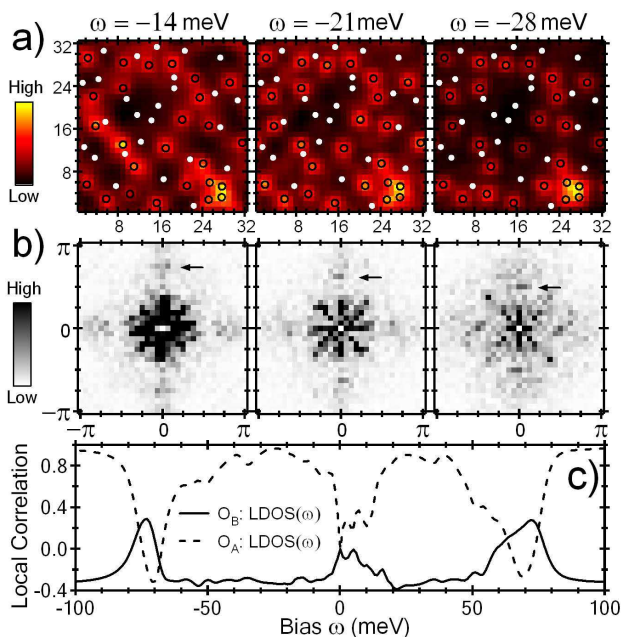


FIG. 3: Electron LDOS maps (a) and the Fourier transform of the quasiparticle interference pattern (b) at low energies. (c) Local correlations of LDOS(i) and the dopant locations as a function of bias energy.

relation of the interference modulations with A-dopants produces a weak *anticorrelation* with the B-dopants as in STM experiments [4]. To further illustrate the interference pattern, the Fourier transform of the quasiparticle LDOS are shown in Fig. 3b at the corresponding energies. The dominant interference wavevector \mathbf{q}_1 (marked by arrows) connecting the tips of the Fermi arcs [23] are clearly seen to disperse with energy near $(0, \pm 2\pi/4a)$ and $(\pm 2\pi/4a, 0)$, while the \mathbf{q}_7 connecting two tips of the same arc shows the opposite dispersion with energy, in remarkable agreement with STM observations [14, 22].

We now provide a possible microscopic origin of the type-A dopants. It is well known that Bi-based cuprates have a natural tendency toward Bi:Sr nonstoichiometry, i.e. a fraction of the Bi comes to the SrO apical plane and replaces the Sr in order to form the crystal structure [24]. This creates the so-called A-site disorder [17, 25]. Since the trivalent Bi^{3+} replacing Sr^{2+} creates an excess positive charge locally, it naturally attracts the negatively charged interstitial oxygen dopants to the vicinity of the apical plane, forming the A-dopants. The doping levels derived from the observed type-B dopants alone are about 5 ~ 6% less than the expected values in the samples studied by McElroy, et.al. [4], suggesting about 5 ~ 6% of the doped holes must come from the ~ 3% “missing” A-dopants. This is reasonably consistent with the typical Bi:Sr nonstoichiometry in Bi2212 where about 5% of the Sr in each apical plane is replaced by Bi [24]. Recently, the effect of A-site disorder on T_c has been

studied systematically by controlled trivalent (Ln^{3+}) substitution of Sr^{2+} in $\text{Bi}_2\text{Sr}_{2-y}\text{Ln}_y\text{CuO}_{6+\delta}$ where $\text{Ln}=\text{La}, \text{Pr}, \text{Nd}, \text{Sm}, \text{Eu}, \text{Gd},$ and Bi [17, 25]. We propose that the STM experiments be carried out on Bi2212 samples with controlled trivalent substitution of Sr in the apical plane. Our theory predicts that the density of the observable type-B dopants would decrease with increasing Ln^{3+} substitution, while that of the type-A dopants increases, leading to stronger electronic disorder.

We have shown that the electrostatic potential of the off-stoichiometric A-dopants can be the primary cause of the electronic disorder and quasiparticle interference modulations observed in $\text{Bi}_2\text{Sr}_2\text{CaCu}_2\text{O}_{8+\delta}$. The electronic inhomogeneity in our theory is driven by that of the kinetic energy or the coherence of doped holes in a doped Mott insulator. Incoherent excitations beyond the Gutzwiller approximation and the dopant induced structural distortions can also contribute to the electronic disorder. We expect such dopant induced electronic disorder in all doped cuprate superconductors, with specific properties dependent on the dopant locations and the crystal field environment, interstitial or substitutional, ordered or disordered. The off-plane dopant structure together with the role of the apical oxygen may account for the varying properties of the cuprates that share, otherwise, identical CuO_2 planes.

We thank J. C. Davis, P. Hirschfeld, W. Ku, D.-H. Lee, P. A. Lee, C. Li, S. H. Pan, and S. Uchida for discussions. This work is supported by DOE grant DE-FG02-99ER45747, ACS 39498-AC5M, and NSF DMR-0353108. ZW thanks the KITP at UCSB for hospitality and acknowledges the support of NSF grant PHY94-07194.

-
- [1] S.H. Pan, et.al. *Nature* **413**, 282 (2001).
 - [2] C. Howald, et.al. *Phys. Rev. B* **64**, 100504 (2001).
 - [3] K.M. Lang, et. al. *Nature* **415**, 412 (2002).
 - [4] K. McElroy, et. al. *Science* **309**, 1048 (2005).
 - [5] A.C. Fang, et. al., *Phys. Rev. Lett.* **96**, 017007 (2006).
 - [6] Y. Kohsaka, et. al. *Phys. Rev. Lett.* **93**, 097004 (2004).
 - [7] T. Hanaguri, et. al. *Nature* **430**, 1001 (2004).
 - [8] H. Mashima, et. al. *Phys. Rev. B* **73**, 060502 (2006).
 - [9] Z. Wang, et. al. *Phys. Rev. B* **65**, 064509 (2002).
 - [10] Q.-H. Wang, J.H. Han, and D.-H. Lee, *Phys. Rev. B* **65**, 054501 (2002).
 - [11] I. Martin and A.V. Balatsky, *Physica C* **357**, 46 (2001).
 - [12] M. Cheng and W.P. Su, *Phys. Rev. B* **72**, 094512 (2005).
 - [13] T.S. Nunner, et. al. *Phys. Rev. Lett.* **95**, 177003 (2005).
 - [14] K. McElroy, et. al. *Phys. Rev. Lett.* **94**, 197005 (2005).
 - [15] G. Baskaran, Z. Zhou, and P.W. Anderson, *Solid State Commun.* **63**, 973 (1987).
 - [16] D. Rokhsar and S. Kivelson, *Phys. Rev. Lett.* **61**, 2376 (1988).
 - [17] K. Fujita, et. al. *Phys. Rev. Lett.* **95**, 097006 (2005).
 - [18] P. Richard, et. al., *Phys. Rev. B* **74**, 094512 (2006).
 - [19] M.R. Norman and H. Ding, *Phys. Rev. B* **57**, R11089 (1998).

- [20] F.C. Zhang, et. al., Supercond. Sci. Technol. **1**, 36 (1988).
- [21] C. Li, S. Zhou, and Z. Wang Phys. Rev. B**73**, 060501 (2006).
- [22] K. McElroy, et. al. Nature **422**, 520 (2003).
- [23] Q.-H. Wang and D.-H. Lee, Phys. Rev. B**67**, 020511 (2003).
- [24] T. Watanabe, et. al., Phys. Rev. Lett. **79**, 2113 (1997).
- [25] H. Eisaki, et. al., Phys. Rev. B**69**, 064512 (2004).